Robotica (2025), **43**, pp. 3657–3681
doi:10.1017/S026357472510249X

CAMBRIDGE UNIVERSITY PRESS

RESEARCH ARTICLE

Configuration design and assisting effect evaluation of a novel double-support closed-chain unpowered load-carrying exoskeleton based on variable pivot gait

Cunjin Ai[1,2,3], Jianjun Zhang[1,3,4], Jun Wei[1,3,4], Jingke Song[1,3,4], Chenglei Liu[1,3,4] and Anyu Shi[1,3,4]

[1]School of Mechanical Engineering, Hebei University of Technology, Tianjin, 300401, China
[2]School of Intelligent Manufacturing Engineering/Automotive Engineering, Chongqing University of Arts and Sciences, Chongqing, 402160, China
[3]Intelligent Rehabilitation Device and Detection Technology Engineering Research Center of the Ministry of Education, Tianjin, 300401, China
[4]Hebei Provincial Key Laboratory of Robot Perception and Human–Machine Fusion, Tianjin, 300401, China
Corresponding authors: Jianjun Zhang; Email: zhjjun@hebut.edu.cn, Jun Wei; Email: jun.wei@hebut.edu.cn

Received: 9 January 2025; **Revised:** 1 July 2025; **Accepted:** 17 August 2025; **First published online:** 7 October 2025

Keywords: variable pivot gait; unpowered exoskeleton; double-support closed-chain; load-carrying

Abstract

Based on the characteristics of the variable pivot gait during the human load-carrying, this paper proposes a double-leg coordination assistance principle for load-carrying: assisting support of the guiding leg at the heel-pivot stage by the spring to reduce the collision, which can reduce the ankle moment of the following leg that is performing the push-off at the toe-pivot stage. A novel unpowered load-carrying exoskeleton (ULE) with a double-support closed-chain configuration is designed, and the theoretical verification is carried out. Five subjects participate in the load-carrying and metabolic cost experiments for assisting and energy-saving effect evaluation, and the angle and moment of human joints, plantar pressure, spring compression and human net metabolic rate are analyzed. Compared with carrying load by the human alone, wearing the novel ULE with spring reduces the human peak ankle moment performing the push-off by up to 11.9 ± 1.6% (Mean±SE, 10 kg), average ankle moment over the support phase by up to 36.8 ± 9.1% (Mean±SE, 5 kg) and the average vertical plantar pressure by up to 8.1 ± 1%% (Mean±SE, 15 kg). Meanwhile, wearing the novel ULE reduces the human net metabolic rate by 5.6 ± 0.5% (Mean±SE, 10 kg), 4.1 ± 0.7% (Mean±SE, 15 kg) and 5.9 ± 1.6% (Mean±SE, 20 kg). The results show that the novel ULE can provide support and joint moment assistance over the whole support phase while reducing human net metabolic rate. This study can also be applied to the powered load-carrying exoskeleton, providing a new avenue.

1. Introduction

Load-carrying is one of the important activities in human life, which has been concerned by researchers. Studies have shown that the kinematics, kinetics, plantar pressure and energy expenditure of the human are all affected when walking with a heavy load [1–3]. With the increase of the load, the spatio-temporal proportion of the support phase in gait, the lower limb joint moment, the plantar pressure, and the energy metabolism all increase [4, 5]. The changes make the human body extremely prone to fatigue, which in turn can trigger the risk of injury or illness.

To assist human load-carrying, researchers have developed a series of auxiliary equipment. Improving the backpack device to redistribute the load on the upper limbs can reduce the stress on the lower limbs, which has limited effectiveness and can easily increase metabolic energy [6, 7]. Powered load-carrying exoskeleton (PLE) can transfer the load to the ground for support and joint assistance. However, PLEs

© The Author(s), 2025. Published by Cambridge University Press.

https://doi.org/10.1017/S026357472510249X Published online by Cambridge University Press

generally require external energy and drive devices, which greatly limit their usage scenarios due to large self-weight and short endurance [8–10]. Flexible joint exoskeletons have a small self-weight and can assist joint moment, but due to the lack of a rigid lower limb structure, they do not have a support assistance function [11, 12]. Supernumerary limb robot has a support structure independent of human legs, which can effectively assist in supporting the load [13, 14]. However, the coordination between the supernumerary limbs and the human legs is difficult to implement [15, 16]. The unpowered load-carrying exoskeleton (ULE) transfers the load to the ground for support assistance by rigid structure, and recovers the energy for joint moment assistance through elastic components or lightweight hydraulic systems [17, 18]. Because there is no external energy or driving device, ULE has the characteristics of light-weight and long-endurance [19, 20].

While ULE provides a new idea for human load-carrying assistance, its design still faces two important challenges. One challenge is gait adaptability. There are many methods for dividing human gait in current exoskeleton research. When the foot is not considered, the support phase is divided into the single-support and double-support phases [21–23]. Because the feet are not considered, this gait is not applicable to ULE. When the feet are considered, papers [24–26] subdivide the single-support and double-support phases according to the contact conditions between the foot and ground, and ignore the stage when the heel of one foot and the toe of the other are in contact with the ground at the same time. In this stage, both feet are not in full contact with the ground, and the spatio-temporal proportion of this stage in the gait cycle increases with the increase of load [27]. This stage can be neglected in PLE because the human joint moments can be compensated by external energy. However, ULE is completely driven by the human lower limbs. Ignoring this stage will cause the loss of key information, such as motion and force between the foot and ground, resulting in a significant impact of elastic elements on human gait. Ultimately, the effect of support and joint moment assistance can not meet expectations. Previous studies indicate that the motion between the foot and ground can be considered as rolling around specific pivots [28, 29]. From the heel touching the ground, the foot rolls forward around the heel pivot, ankle pivot (ankle joint), forefoot pivot (metatarsophalangeal joint) and toe pivot in turn. Based on this, a variable pivot gait (VPG) is proposed in our previous study [30]. This gait contains the stage when the heel of one foot and the toe of the other are in contact with the ground at the same time, which can completely describe the actual situation of contact conditions between the foot and ground.

Another challenge is the design of assistance principle. Push-off plays a crucial role in normal human walking gait [31, 32]. Direct assist to the ankle joint by elastic elements during the push-off has always been a focus of unpowered assisting walking exoskeletons [33, 34]. However, there are no cases of applying this method to ULE. Papers [35, 36] point out that there is a coordination between the ankle push-off of the following leg and the heel collision of the guiding leg during walking. When the push-off work decreases, the collision work needs to be increased to achieve the reorientation of the body centroid speed during the step-to-step transition.

The main contribution of this paper is that, based on VPG, a double-leg coordination assistance principle for load-carrying is proposed: assisting support of the guiding leg to reduce the collision to reduce the ankle moment of the following leg that is performing the push-off. Meanwhile, a novel ULE with a double-support closed-chain configuration is designed, and the assistance principle is verified by experiments for assisting and energy-saving effect evaluation.

The paper is organized as follows: In Section 2, the corresponding gait stages of push-off and collision in VPG are determined through human load-carrying experiments, and an assisting principle for load-carrying is proposed. Based on the principle, a novel ULE with a double-support closed-chain configuration is designed, and relevant theories are verified. In Section 3, load-carrying experiments are conducted with 0, 5, 10, 15 and 20 kg load, respectively, under the three conditions of without ULE, wearing ULE without spring and with spring. In Section 4, the plantar pressure, spring compression, angle and moment of human joints during the experiment are analyzed. In Section 5, metabolic cost experiment and result analysis are conducted with 0, 5, 10, 15 and 20 kg load under the three conditions. Sections 6 and 7 are discussion and conclusion, respectively.

https://doi.org/10.1017/S026357472510249X Published online by Cambridge University Press

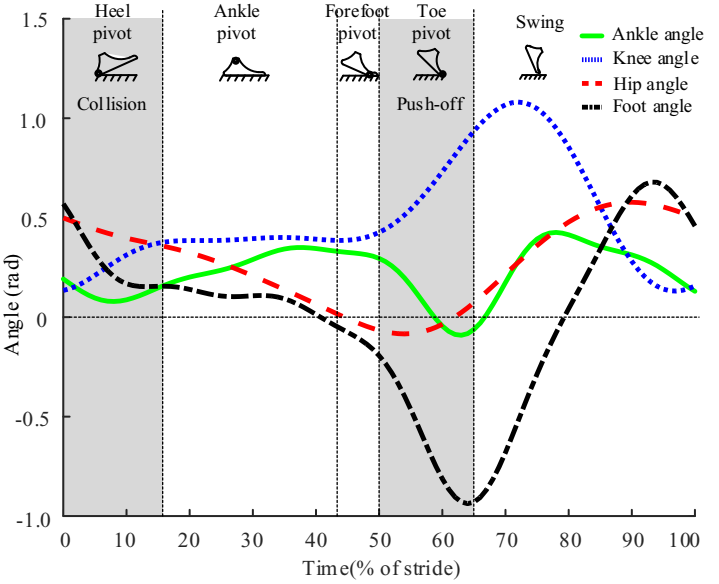


Figure 1. *Kinematic parameters of human low limb with 10 kg load. The foot angle was the angle between the hindfoot and the ground at normal walking speed(cadence, 60 steps/min). Data shown were trajectories averaged across subjects (N = 5).*

2. Assistance principle, configuration design and dynamics analysis of the novel ULE

2.1. Assistance principle for load-carrying

The kinematics of the human lower limbs with a 10 kg load is shown in Figure 1. The analysis indicates that the heel of one foot (heel-pivot stage, 0–15%) and the toe of the other (toe-pivot stage, 50–65%) are in contact with the ground synchronously. The heel-pivot stage mainly performs collision function, while the toe-pivot stage mainly performs push-off function.

The human VPG model is shown in Figure 2 when collision and push-off functions are considered. The single-leg (red rod) support phase of the human body is subdivided into: double-support heel-pivot stage, single-support ankle-pivot stage, single-support forefoot-pivot stage and double-support toe-pivot stage. Based on VPG, the assistance principle for load-carrying is proposed as follows: (1) Double-support phase, assisting support of the guiding leg at the heel-pivot stage, directly reducing the force on the lower limb during heel collision, assisting the reorientation of the load centroid, thus reducing the ankle joint moment of the following leg that is performing the push-off function at the toe-pivot stage; (2) Single-support phase, the load of the support leg is transferred to the ground for support and joint moment assistance.

2.2. Design of ULE with a double-support closed-chain configuration

Based on the assistance principle, a novel ULE with a double-support closed-chain configuration is proposed, which is shown in Figure 3. The ULE consists of a symmetrical left and right closed-chain support mechanism and a backpack. The two closed-chain support mechanisms are connected to the backpack through an abductor joint, as shown in Figure 3(a). As shown in Figure 3(b), the unilateral closed-chain support mechanism has 3 freedoms, which are composed of the anterior and posterior branch chains connected through the connecting bars and the luggage carriers. The anterior branch chain is bound to the human thigh, shank and foot, which is driven by the human hip, knee and ankle joints. As shown in Figure 3(c), the posterior branch chain has two rotational joints, and there is a prismatic joint arranged with a linear spring at the support bar, and the length regulator makes the ULE adapt to

https://doi.org/10.1017/S026357472510249X Published online by Cambridge University Press

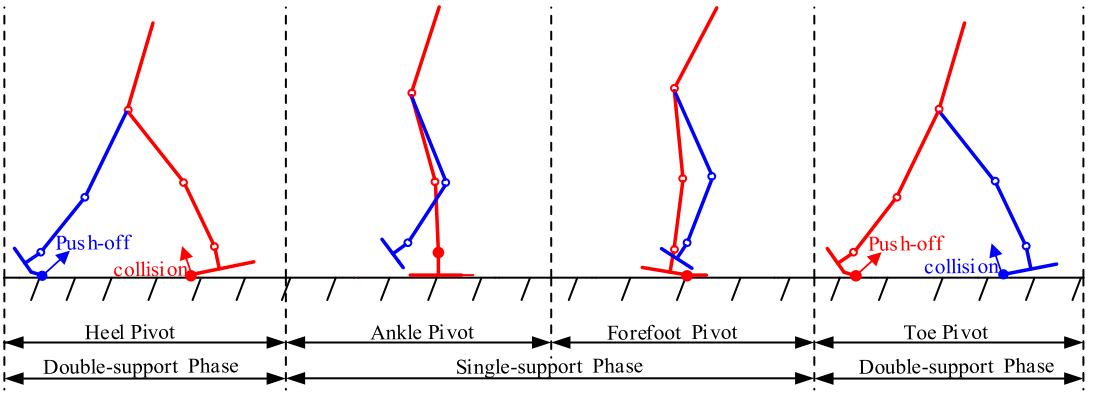


Figure 2. *Variable pivot gait considering collision and push-off.*

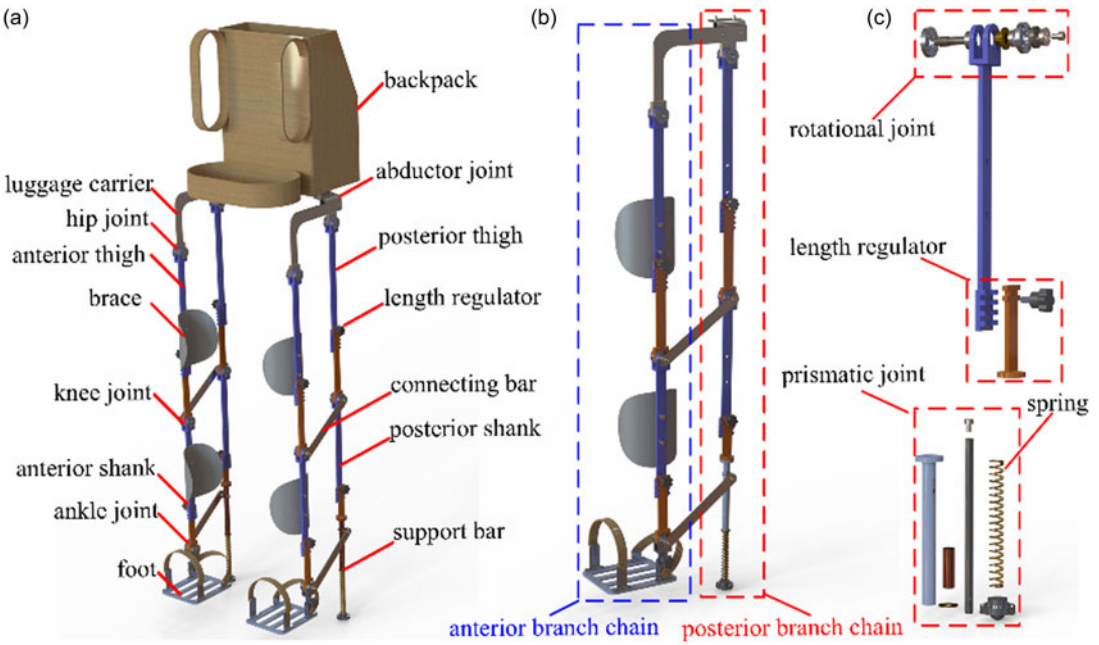


Figure 3. *The novel unpowered load-carrying exoskeleton (ULE). (a) 3D model. (b) Double-supported closed-chain mechanism. (c) Design of length regulator, rotational and prismatic joints.*

the heights of humans from 1680 to 1850 mm. The ULE worn by the human body is shown in Figure 4, with an overall weight (including the backpack) of 5 kg.

The working principle of ULE is shown in Figure 5, which can achieve both support and joint moment assistance during the whole support phase. Joint moment assistance: (1) Double-support phase, when the heel of the right leg marked in red contacts the ground, the spring contacts the ground in advance, converting the collision energy loss into elastic potential energy, thus reducing the energy required for the left leg in the toe-pivot stage to push off the ground and reducing the ankle joint moment as shown in Figure 5(a) and (d); (2) Single-support phase, the posterior branch chain releases the spring force to assist the support leg joint moments as shown in Figure 5(b) and (c). Support assistance: during the whole support phase, when the human foot is in contact with the ground, ULE transfers the load to the ground through the anterior and posterior branch chains to achieve support assistance.

https://doi.org/10.1017/S026357472510249X Published online by Cambridge University Press

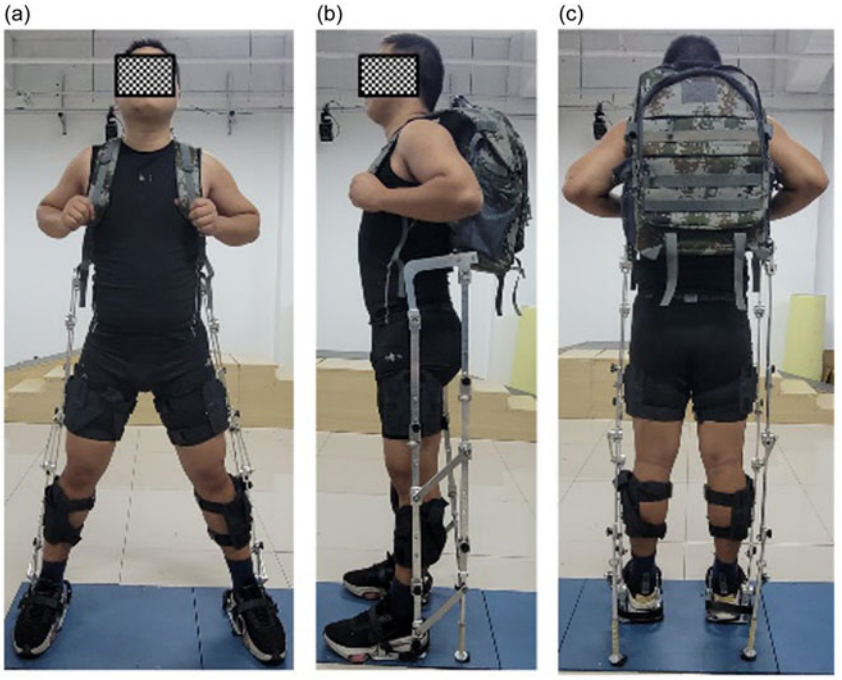


Figure 4. *ULE wearing. (a–c) Front, side and rear views of ULE wearing.*

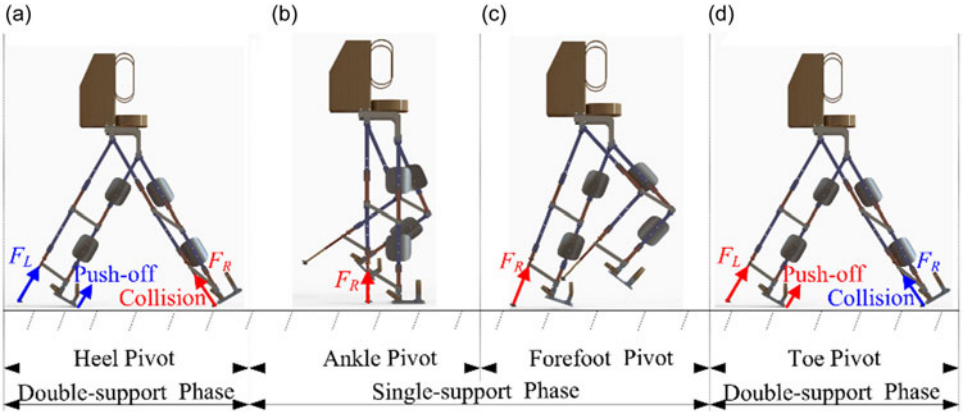


Figure 5. *Principle of ULE. Right leg (marked in red): (a) Heel-pivot stage, support assistance. (b, c) Ankle-pivot and forefoot-pivot stages, support and joint moment assistance. (d) Toe-pivot stage, joint moment assistance.*

2.3. Kinematics and dynamics analysis

The heel-pivot, ankle-pivot, forefoot-pivot and toe-pivot stages of unilateral ULE are analyzed, respectively. The closed vector method is used for kinematics calculation, and the Lagrange equations of the second kind are used to calculate the hip, knee and ankle moments required to drive the ULE with or without spring.

Unilateral ULE simplified model is displayed as Figure 6. θ_1, θ_2, θ_3 and θ_0 are the angles of human ankle joint, knee joint, hip joint and foot-ground, respectively. θ *and* θ_4 are constants related to the size of the mechanism. q_5, q_6, q_7 and q_8 are the angles between the corresponding bar and the vertical direction, respectively. The positive and negative definitions of angles are marked in Figure 6. A_0 is the origin of the coordinate system. l_g is the distance from heel to ankle, and l_q is the distance from the ankle to the

https://doi.org/10.1017/S026357472510249X Published online by Cambridge University Press

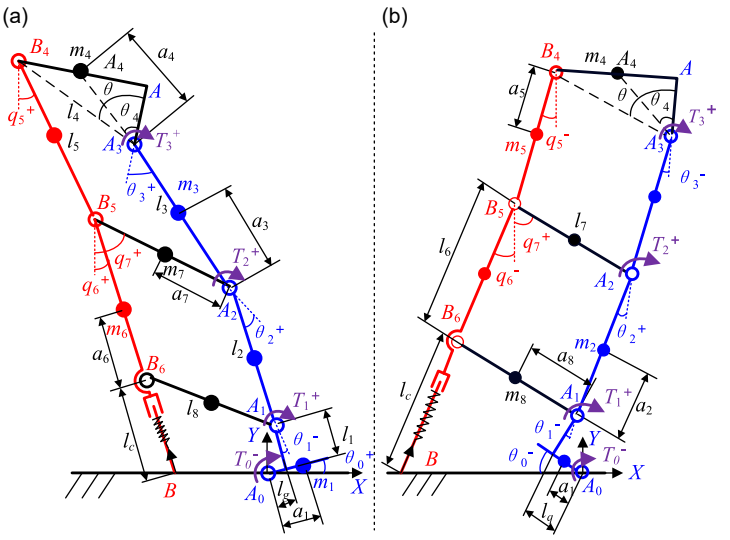


Figure 6. *Unilateral ULE simplified model. (a) Heel-pivot and ankle-pivot stage model. (b) Forefoot-pivot and toe-pivot stage model.*

forefoot-pivot or toe-pivot. l_i is the length of each bar, a_i is the distance of the centroid, $i = 1, 2, 3,\ldots, 8$; meanwhile, $l_2 = l_6$, $l_3 = l_5$, $l_4 = l_7 = l_8$.

2.3.1. Kinematics analysis

Kinematic analysis of parallelogram $A_2A_3B_4B_5$ and $A_0A_1B_6B$ can be obtained:

$$\begin{bmatrix} q_1 \\ q_2 \\ q_3 \\ q_4 \\ q_5 \\ q_6 \\ q_7 \\ q_8 \end{bmatrix} = \begin{bmatrix} 1 & 0 & 0 & 0 & 0 & 0 \\ 1 & -1 & 0 & 0 & 0 & 0 \\ 1 & -1 & 1 & 0 & 0 & 0 \\ 1 & -1 & 1 & -1 & 1 & 0 \\ 1 & -1 & 1 & 0 & 0 & 0 \\ 1 & -1 & 0 & 0 & 0 & 0 \\ 1 & -1 & 1 & -1 & 0 & 1 \\ 1 & -1 & 1 & -1 & 0 & 1 \end{bmatrix} \begin{bmatrix} \theta_0 \\ \theta_1 \\ \theta_2 \\ \theta_3 \\ \theta_4 \\ \theta \end{bmatrix} \tag{1}$$

The l_c change represents the compression of the spring inside the support bar. The spring compression Δl can be obtained:

$$l_c = \frac{l_g \sin\theta_0 + l_1 \cos\theta_0 + l_8 \cos(\theta + \theta_0 - \theta_1 + \theta_2 - \theta_3)}{\cos(\theta_0 - \theta_1)} \tag{2}$$

$$\Delta l = l_c - l_{c0} \tag{3}$$

In Eq. (3), l_{c0} and l_c are the original and real-time length of the support bar, respectively.

The coordinates of the centroid of each bar during support phase are obtained:

$$\begin{bmatrix} x_1 \\ x_2 \\ x_3 \\ x_4 \\ x_5 \\ x_6 \\ x_7 \\ x_8 \end{bmatrix} = \begin{bmatrix} a & 0 & 0 & 0 & 0 & 0 & 0 & 0 \\ b & -l_1 & -a_2 & 0 & 0 & 0 & 0 & 0 \\ b & -l_1 & -l_2 & -a_3 & 0 & 0 & 0 & 0 \\ b & -l_1 & -l_2 & -l_3 & -a_4 & 0 & 0 & 0 \\ b & -l_1 & -l_2 & 0 & 0 & -a_5 & 0 & -l_7 \\ b & -l_1 & 0 & 0 & 0 & 0 & -a_6 & -l_8 \\ b & -l_1 & -l_2 & 0 & 0 & 0 & 0 & -a_7 \\ b & -l_1 & 0 & 0 & 0 & 0 & 0 & -a_8 \end{bmatrix} \begin{bmatrix} \cos\theta_0 \\ \sin\theta_0 \\ \sin(\theta_0 - \theta_1) \\ \sin(\theta_0 - \theta_1 + \theta_2) \\ \sin(\theta_0 - \theta_1 + \theta_2 - \theta_3 + \theta_4) \\ \sin(\theta_0 - \theta_1 + \theta_2) \\ \sin(\theta_0 - \theta_1) \\ \sin(\theta_0 - \theta_1 + \theta_2 - \theta_3 + \theta) \end{bmatrix} \tag{4}$$

https://doi.org/10.1017/S026357472510249X Published online by Cambridge University Press

$$\begin{bmatrix} y_1 \\ y_2 \\ y_3 \\ y_4 \\ y_5 \\ y_6 \\ y_7 \\ y_8 \end{bmatrix} = \begin{bmatrix} a & 0 & 0 & 0 & 0 & 0 & 0 & 0 \\ b & l_1 & a_2 & 0 & 0 & 0 & 0 & 0 \\ b & l_1 & l_2 & a_3 & 0 & 0 & 0 & 0 \\ b & l_1 & l_2 & l_3 & a_4 & 0 & 0 & 0 \\ b & l_1 & l_2 & 0 & 0 & a_5 & 0 & l_7 \\ b & l_1 & 0 & 0 & 0 & 0 & a_6 & l_8 \\ b & l_1 & l_2 & 0 & 0 & 0 & 0 & a_7 \\ b & l_1 & 0 & 0 & 0 & 0 & 0 & a_8 \end{bmatrix} \begin{bmatrix} \sin\theta_0 \\ \cos\theta_0 \\ \cos(\theta_0 - \theta_1) \\ \cos(\theta_0 - \theta_1 + \theta_2) \\ \cos(\theta_0 - \theta_1 + \theta_2 - \theta_3 + \theta_4) \\ \cos(\theta_0 - \theta_1 + \theta_2) \\ \cos(\theta_0 - \theta_1) \\ \cos(\theta_0 - \theta_1 + \theta_2 - \theta_3 + \theta) \end{bmatrix} \tag{5}$$

In Eqs. (4) and (5), during heel-pivot and ankle-pivot stage, $a = a_1$, $b = l_g$; during forefoot-pivot and toe-pivot stage, $a = -a_1$, $b = -l_q$.

2.3.2. Dynamics analysis

As shown in Figure 6, T_1, T_2 and T_3 are the drive moments of the anterior branch chain, and T_0 is the moment required between the foot and the ground. Taking θ_0, θ_1, θ_2 and θ_3 as generalized coordinates, the total kinetic energy and potential energy of the system are expressed as follows:

$$K = \frac{1}{2}\sum_{i=1}^{8}\left[I_i\dot{q}_i^2 + m_i\left(\dot{x}_i^2 + \dot{y}_i^2\right)\right] \tag{6}$$

$$P = \sum_{i=1}^{8} m_i g y_i + \frac{1}{2}k\Delta l^2 \tag{7}$$

$\dot{q}_i$ is the absolute angular velocity of each bar to the ground, I_i is the rotational inertia, m_i is the mass, $\dot{x}_i$ and $\dot{y}_i$ are the velocities of the centroid, $n = 8$. g is the acceleration of gravity and k is the spring stiffness.

The Lagrange function of the human lower limbs system is defined as follows:

$$L = K - P \tag{8}$$

$$T_i = \frac{d}{dt}\left[\frac{\partial L}{\partial \dot{\theta}_i}\right] - \frac{\partial L}{\partial \theta_i} \tag{9}$$

2.3.3. Kinematics and dynamics calculation results

Assuming that ULE does not interfere with the motion of the human with load-carrying, the joint angle of the human lower limbs in Figure 1 is used as the motion input of the ULE for dynamics calculation. The principles for determining ULE scale parameters are as follows: (1) the bar length is based on the human at 1710 mm refer to ref. [37]; (2) the spring stiffness $k = 2$ N/mm is determined by the principle that the posterior branch chain shares half of the load when the human body is standing static. $l_4 = l_7 = l_8 = 180$ mm, $l_{c0} = 170$ mm.

As shown in Figure 7(a) and (d), the spring has a significant assistance on the ankle moment at both the ankle-pivot and forefoot-pivot stages of unilateral ULE. Meanwhile, the spring also has a certain assisting effect on the knee and hip joints, as shown in Figure 7(b) and (c). The assisting effect of the combined action of both legs needs to be measured by load-carrying experiment.

3. Load-carrying experiments

3.1. Experiment and measurement protocols

We conducted load-carrying experiments on 5 healthy subjects under three conditions: without ULE (WU), wearing ULE without spring (UOS), and wearing ULE with spring (UWS). These conditions are shown in Figure 8, respectively. All subjects received explanations about the nature and possible consequences of the experiments before their participation. The study was approved by the Biomedical

https://doi.org/10.1017/S026357472510249X Published online by Cambridge University Press

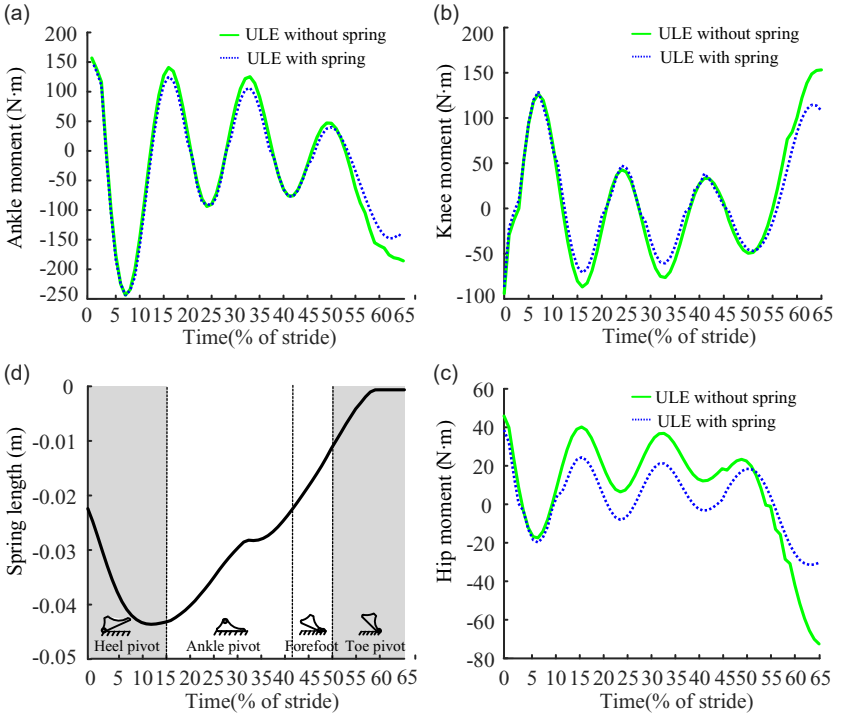


Figure 7. *Joint moments and spring compression of ULE at support phase. (a–c) Hip, knee and ankle moments required to drive ULE with and without spring. (d) Spring compression.*

Ethics Committee of Hebei University of Technology in Tianjin, China. The ethics protocol number: HEBUTHMEC2025040. Table I lists the details of the 5 male subjects ($N = 5$).

The experiment protocol was separated into training and testing. In the training, the subjects under each condition with 4 loads (5, 10, 15 and 20 kg) walked on the ground, respectively. With the metronome, each training cadence was 60 steps/min, and the time was 5 min. In the testing, each subject under each condition with 4 loads (5, 10, 15 and 20 kg) walked on the force platforms at 60 steps/min cadence per trial. The criterion for the success of per trial: the left leg steps onto the first force platform, the right foot steps onto the second force platform and then the left leg steps onto the third force platform. The 8 results of a load test under each condition are averaged. When ULE was worn with a spring, the spring parameters corresponding to each load were shown in Table II, in which 0 kg without spring is the control group.

Motions were measured by a reflective marker motion capture system (10 cameras, Nokov, Beijing Metrology Technology Co., Ltd., China; 100 Hz). The reflective balls were placed according to the 39-point rule of 2392 human model, as referred to in ref. [38]. Reflective balls at the joint position were easily obscured by the exoskeleton; therefore, 1 cm reflective balls were used, and 1.5 cm reflective balls were used for the rest positions, as shown in Figure 9(c) and (d). In addition, the reflective balls are arranged at the prismatic joint at both ends of the support bar to obtain the spring compression.

The total ground reaction force of the human and ULE was measured by 3 force platforms (AMTI, Watertown, MA, USA; 90∗60 cm; 100 Hz). When the human was wearing ULE, the plantar pressure of the human was collected by the pressure insole (RX-ES42-18, CROWNTO, Luoyang crown extension electronic Co., Ltd., China) as shown in Figure 9(a) and (b).

3.2. Experiment data processing and analysis

Human body scaling must be performed based on each subject's static data before inverse kinematics (IK), ensuring subsequent motion data can be used for calculations according to the subjects' actual

https://doi.org/10.1017/S026357472510249X Published online by Cambridge University Press

Table I. *Parameters of 5 subjects.*

Subject number	Height (mm)	Weight (kg)	Age (years)
1	1680	78	27
2	1760	75	20
3	1700	65	20
4	1810	77	24
5	1715	80	35
Mean±SD	1733 ± 52.2	75 ± 5.9	25.2 ± 6.2

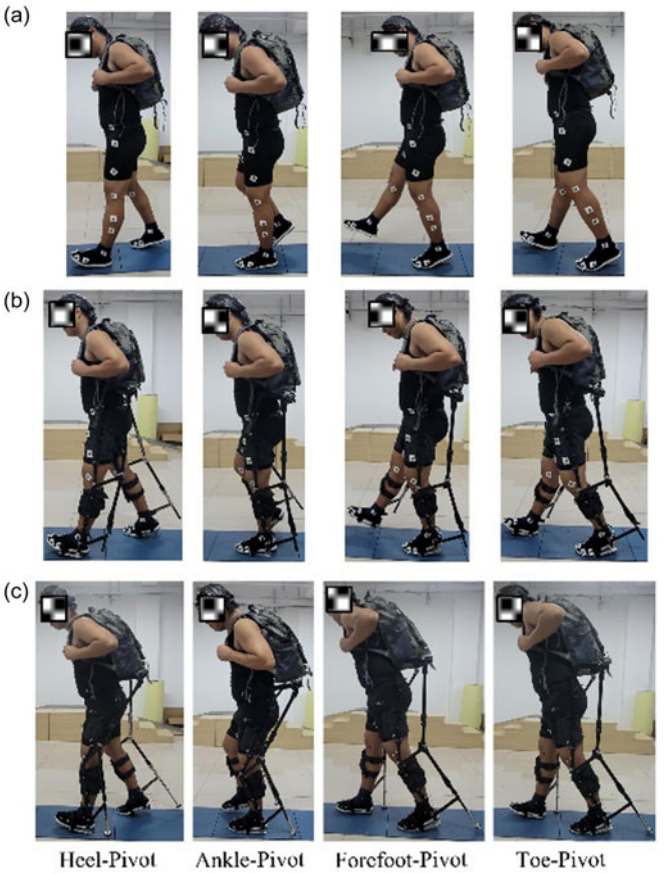


Figure 8. *Load-carrying experiments for assisting effect evaluation. (a) Without ULE (WU). (b) Wearing ULE without spring (UOS). (c) Wearing ULE with spring (UWS).*

body parameters. First, MATLAB (MATLAB 2018b, Mathworks, USA) converts the static C3D-format human body data collected in the static experiment into TRC-format. Then, the converted TRC static data, virtual marker setting file and scaling setting file are imported based on OpenSim (OpenSim4.2, Stanford University, USA) standard Gait2392 model. Finally, OpenSim scaling tool adjusts the corresponding virtual markers in the Gait2392 model from bottom to top, prioritizing positions with the largest errors between experimental and virtual markers. Human body scaling is completed when the maximum error of bone markers is less than 2 cm and the root mean square error (RMS) is less than 1 cm, the human body scaling is completed.

After scaling the human body model, exoskeleton rod lengths are adjusted according to human bone joint feature dimensions. Using Notepad++(Version 7.4.2, Kim JongDaehyun, ROK) for programing,

https://doi.org/10.1017/S026357472510249X Published online by Cambridge University Press

Table II. *Spring parameters corresponding to each load.*

Spring model	Length (mm)	Max load (kg)	Stiffness (N/mm)	Load(kg)
SWY16.5-125	125	9.1	1.08	5
SWR14.5-125	125	12.8	2.04	10
SWR17-125	125	19.6	3.14	15
SWR18-125	125	25.5	4.1	20
Control				0

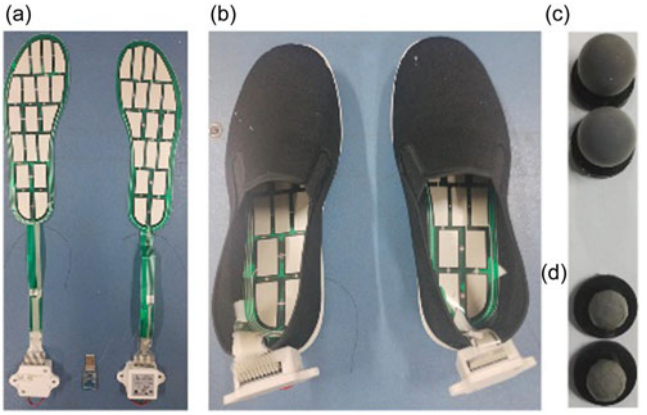


Figure 9. *Pressure insole and marks. (a) Pressure insoles with bluetooth receiver. (b) Pressure insoles arrangement. (c) 1.5 reflective balls. (d) 1 cm reflective balls.*

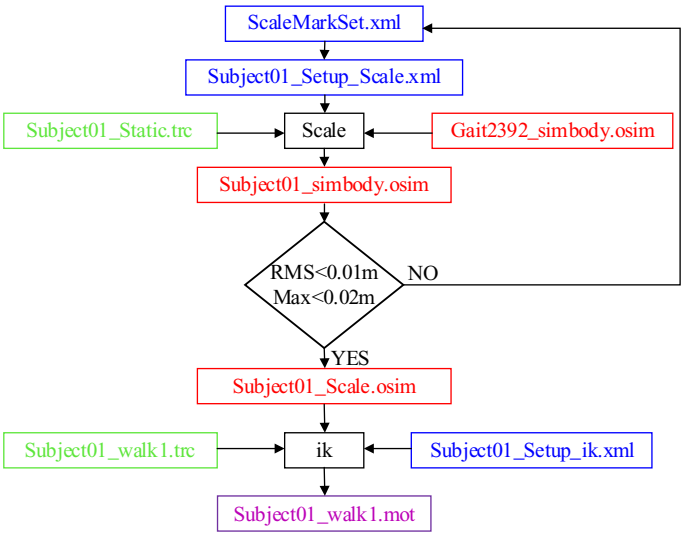


Figure 10. *Scaling and inverse kinematics process.*

each rod is imported into the scaled Gait2392 model to generate a human–machine coupling model corresponding to each subject wearing the exoskeleton. Following scaling, OpenSim IK algorithm solves the human–machine IK problem, converting motion marker data from the human–machine loaded motion capture experiment into actual lower limb joint angles. The scaling and IK process is illustrated in Figure 10.

The scaling and IK were calculated by OpenSim software to obtain the angles of human lower limb joints [39, 40]. The calculation of joint moments in the sagittal plane was based on the human–machine

https://doi.org/10.1017/S026357472510249X Published online by Cambridge University Press

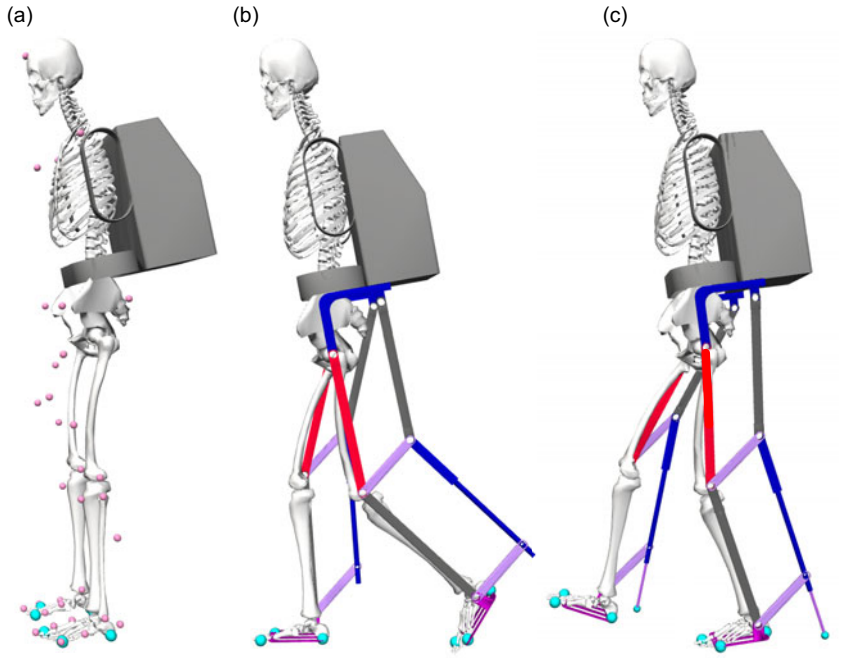


Figure 11. *OpenSim human–machine coupling simulation model. (a) Without ULE (WU). (b) Wearing ULE without spring (UOS). (c) Wearing ULE with spring (UWS).*

coupling model developed by OpenSim, as shown in Figure 11. The Moco algorithm module in OpenSim was used to track the joint motions and plantar forces collected in the experiment [41, 42], and the joint moments of the human lower limbs were obtained through MATLAB programing and calculation.

The average and standard deviations of human plantar pressure, spring compression, angle and moment of human lower limb joints were calculated ($N = 5$) for each load under the three conditions. Meanwhile, statistical analysis was performed using GraphPad Prism (version 9.5, GraphPad Software, San Diego, California, USA). The peak, averages during whole stride and support phase of the joint moments (hip, knee and ankle) and plantar pressure for each load under the three conditions were analyzed by one-way repeated measures analysis of variance (ANOVA). Furthermore, the Bonferroni post hoc test was performed to determine the level of significant difference between conditions and verify support and joint moment assistance of ULE.

4. Results of load-carrying experiments for assisting effect evaluation

4.1. Joint kinematics

The kinematics results of the human carrying 5 loads (0, 5, 10, 15 and 20 kg), respectively, under the three conditions are shown in Figure 12. As shown in Figure 12(a), (f) and (k), UOS with 0 kg load has little impact on human lower limb motions. With the increase of load, the spatiotemporal proportion of the double support phase (heel-pivot and toe-pivot stages) in the gait cycle and the ankle plantarflexion angle in the toe-pivot stage increase continuously. Meanwhile, UWS can effectively reduce the ankle plantarflexion angle compared with WU in the toe-pivot stage, as shown in Figure 12(k−o). In addition, with the load increasing, the impact of UOS on human motions increases, as shown in Figure 12(e), (j) and (o).

4.2. Joint moments

4.2.1. Ankle, knee and hip joint moments with 5 kg load

With 5 kg load, the trajectories of ankle, knee and hip moments in three conditions are shown in Figure 13(a), (e) and (i). The trends of the ankle moments among three conditions are almost the same, as

https://doi.org/10.1017/S026357472510249X Published online by Cambridge University Press

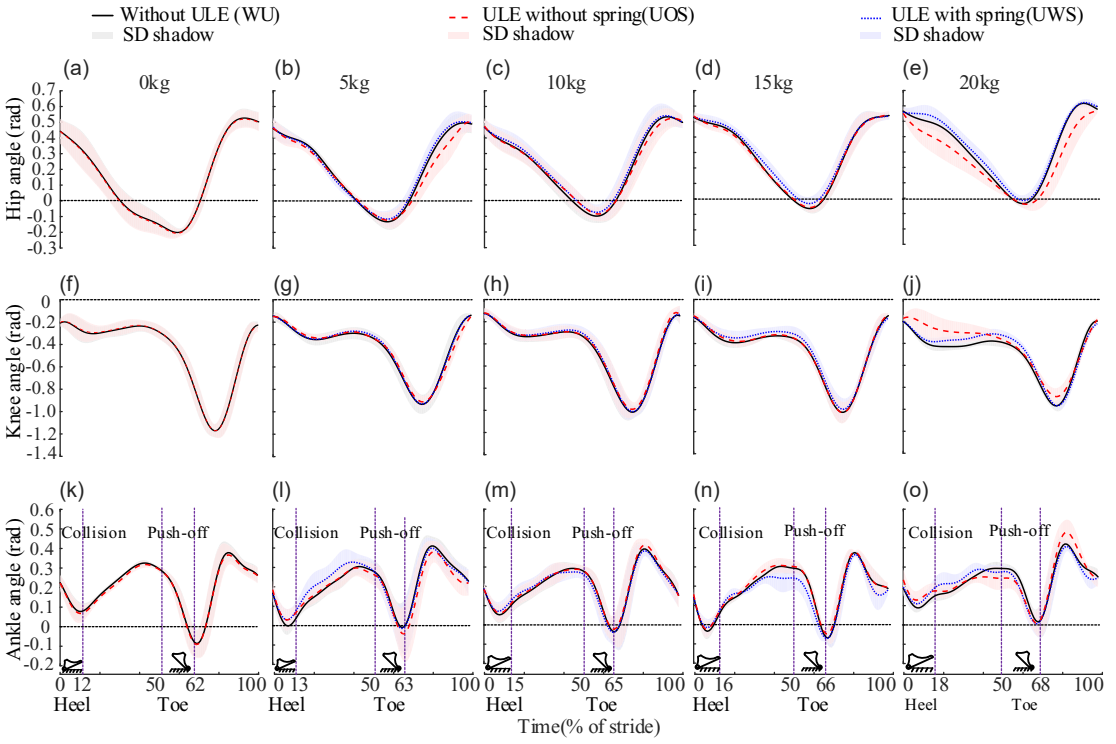


Figure 12. *Hip, knee and ankle joint angles. (a–e) Hip joint angles, (f–j) knee joint angles, and (k-o) ankle joint angles. Data shown are trajectories averaged across subjects (N = 5), and shadows represent standard deviation (SD).*

shown in Figure 13(a). After the ANOVA test for WU, UOS and UWS as shown in Figure 13(b–d). The average ankle moments over the whole stride and support phase of the three conditions show significant differences ($p = 0.008$, $p = 0.008$). Bonferroni post-hoc test shows that both the average ankle moment over the whole stride and support phase can be reduced in the UWS compared with WU (post-hoc test, $p = 0.04$, $p = 0.05$). The peak ankle moment of the three conditions showed a significant difference ($p < 0.001$), which can be reduced in the UWS compared with WU (post-hoc test, $p = 0.005$).

The ANOVA results also show that UWS has little effect on knee moment, as shown in Figure 13(f–h). Compared with WU, the average knee moments over the whole stride and support phase (post-hoc test, $p > 0.99$, $p > 0.99$), and the peak knee moment (post-hoc test, $p > 0.99$) of UWS have no significant difference. However, compared with WU, the average knee moments over the whole stride and support phase (post-hoc test, $p < 0.001$, $p = 0.01$), and the peak knee moment (post-hoc test, $p = 0.03$) of UOS show that knee moment is increased. As shown in Figure 13(j-l), compared with WU, the hip moment is reduced significantly in UWS, especially the peak hip moment (post-hoc test, $p = 0.04$).

4.2.2. Ankle, knee and hip joint moments with 10 kg load

With 10 kg load, the trajectories of ankle, knee and hip moments in three conditions are shown in Figure 14(a), (e) and (i). The trends of the ankle moments among the three conditions are almost the same as shown in Figure 14(a). After the ANOVA test for WU, UOS and UWS, as shown in Figure 14(b–d). The average ankle moments over the whole stride and support phase of the three conditions show significant differences ($p < 0.001$, $p = 0.001$). Bonferroni post-hoc test shows that both the average ankle moment over the whole stride and support phase can be reduced in UWS compared with WU (post-hoc test, $p = 0.005$, $p = 0.01$). The peak ankle moment of the three conditions showed a significant difference ($p = 0.002$), which can be reduced in the UWS compared with WU (post-hoc test, $p = 0.005$).

https://doi.org/10.1017/S026357472510249X Published online by Cambridge University Press

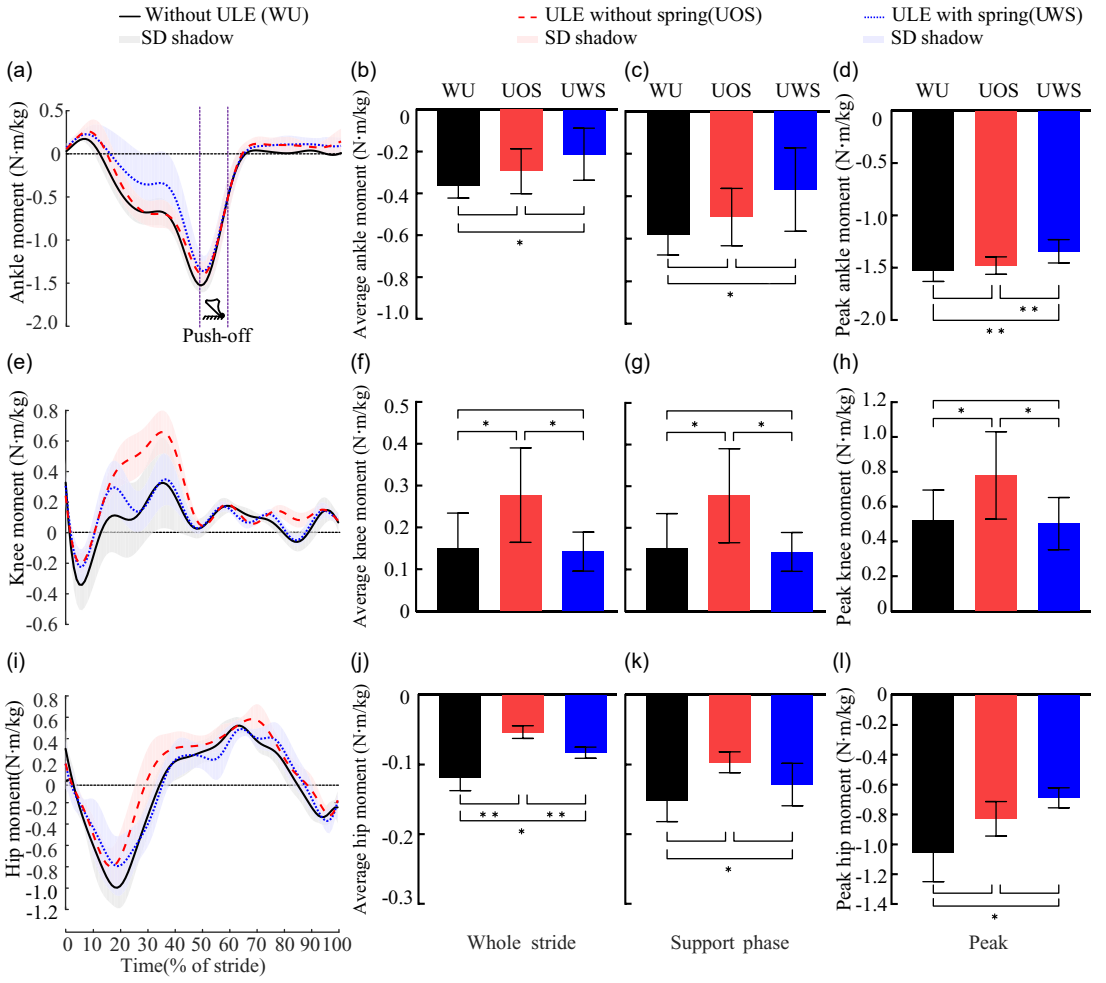


Figure 13. *Ankle, knee and hip joint moments with 5 kg load. (a, e and i) Trajectories of ankle, knee and hip joint moments averaged across subjects (N = 5), and shadows represent standard deviation (SD). (b, c) Average ankle moments over the whole stride and support phase. (d) Peak ankle moment. (f, g) Average knee moments over the whole stride and support phase. (h) Peak knee moment. (j, k) Average hip moments over the whole stride and support phase. (l) Peak hip moment. *Significant difference at $p < 0.05$, **significant difference at $p < 0.01$, ***significant difference at $p < 0.001$; error bars, SD; support phase, 0–63% stride; all the joint moments were normalized to subject body mass.*

The ANOVA results also show that UWS has little effect on knee moment, as shown in Figure 14(f–h). Compared with WU, the average knee moments over the whole stride and support phase (post-hoc test, $p = 0.53$, $p > 0.99$), and the peak knee moment (post-hoc test, $p = 0.15$) of UWS have no significant difference. However, compared with WU, the average knee moment over the support phase and the peak knee moment (post-hoc test, $p = 0.01$, $p = 0.02$) of UOS show that knee moment is increased. As shown in Figure 14(j–l), compared with WU, the hip moment is reduced significantly in UWS, especially the peak hip moment (post-hoc test, $p = 0.02$).

4.2.3. Ankle, knee and hip joint moments with 15 kg load

With 15 kg load, the trajectories of ankle, knee and hip moments in three conditions are shown in Figure 15(a), (e) and (i). The trends of the ankle moments among the three conditions are almost the same

https://doi.org/10.1017/S026357472510249X Published online by Cambridge University Press

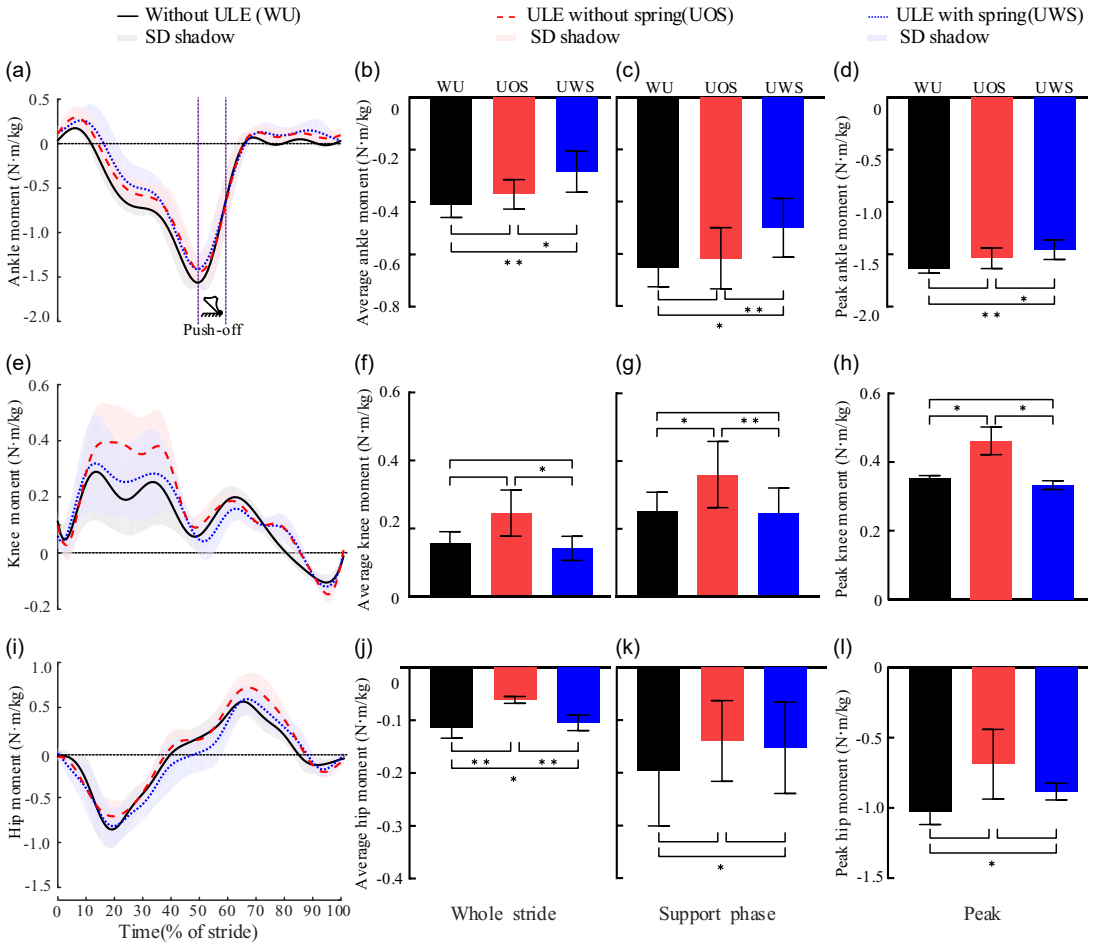


Figure 14. *Ankle, knee and hip joint moments with 10 kg load. (a–j) The meaning of the content in each figure is the same as that in Figure 13. Support phase, 0–65% stride.*

as shown in Figure 15(a). After the ANOVA test for WU, UOS and UWS, as shown in Figure 15(b–d). The average ankle moments over the whole stride and support phase of the three conditions show significant differences ($p = 0.009$, $p < 0.001$). Bonferroni post-hoc test shows that both the average ankle moment over the whole stride and support phase can be reduced in the UWS compared with WU (post-hoc test, $p = 0.02$, $p = 0.001$). The peak ankle moment of the three conditions showed a significant difference ($p < 0.001$), which can be reduced in the UWS compared with WU (post-hoc test, $p < 0.001$).

The ANOVA results also show that UWS has little effect on knee moment, as shown in Figure 15 (f–h). Compared with WU, the average knee moments over the whole stride and support phase (post-hoc test, $p = 0.2$, $p = 0.72$), and the peak knee moment (post-hoc test, $p = 0.06$) of UWS have no significant difference. However, compared with WU, the average knee moment over the support phase and the peak knee moment (post-hoc test, $p = 0.01$, $p = 0.02$) of UOS show that the knee moment is increased. As shown in Figure 15(j–l), compared with WU, the hip moment is reduced significantly in UWS, especially the peak hip moment (post-hoc test, $p = 0.07$).

4.2.4. Ankle, knee and hip joint moments with 20 kg load

With 20 kg load, the trajectories of ankle, knee and hip moments in three conditions are shown in Figure 16(a), (e) and (i). The trends of the ankle moments among the three conditions are almost the same as shown in Figure 16(a). After the ANOVA test for WU, UOS and UWS, as shown in Figure 16(b–d).

https://doi.org/10.1017/S026357472510249X Published online by Cambridge University Press

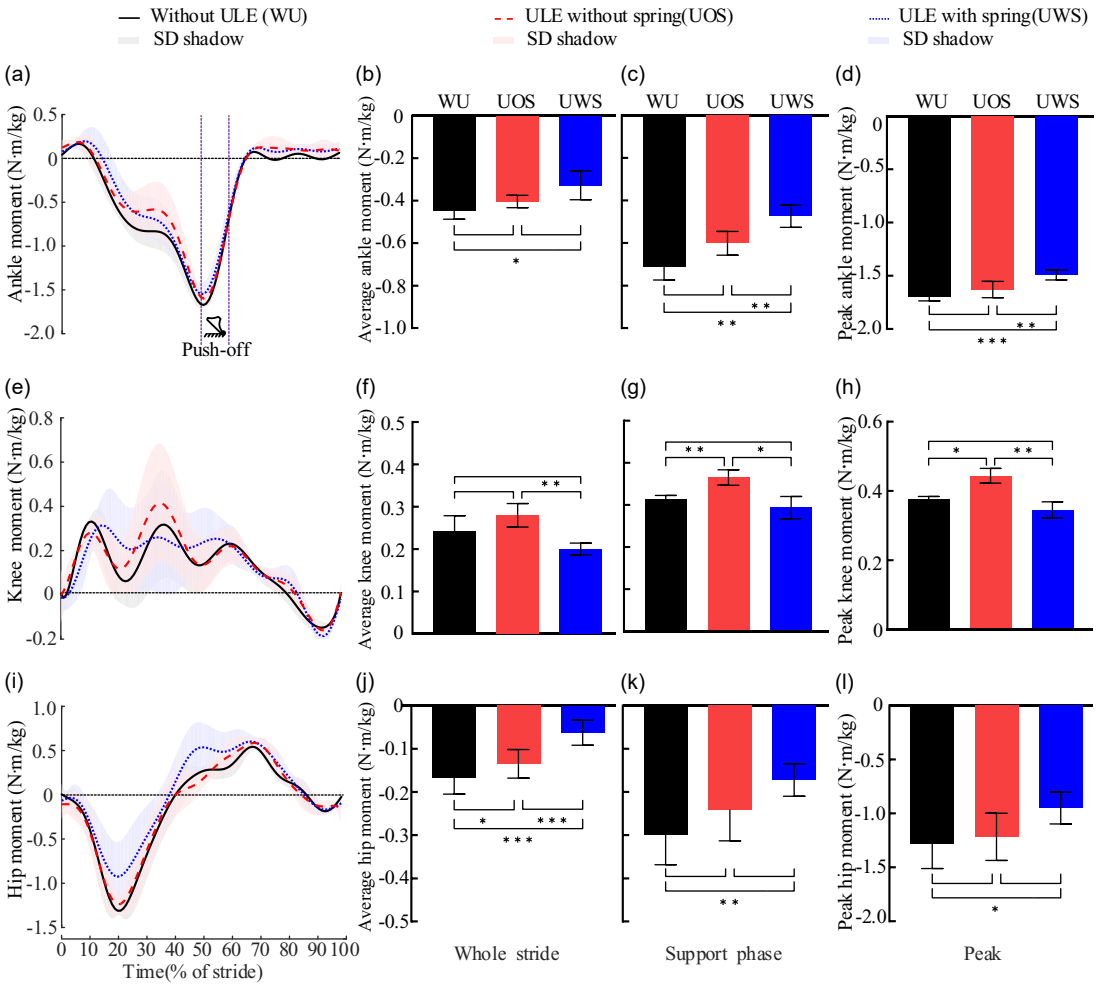


Figure 15. *Ankle, knee and hip joint moments with 15 kg load. (a–j) The meaning of the content in each figure is the same as that in Figure 13. Support phase, 0–66% stride.*

The average ankle moments over the whole stride and support phase of the three conditions show significant differences ($p < 0.001$, $p = 0.03$). Bonferroni post-hoc test shows that both the average ankle moment over the whole stride and support phase can be reduced in the UWS compared with WU (post-hoc test, $p < 0.001$, $p = 0.004$). The peak ankle moment of the three conditions showed a significant difference ($p = 0.004$), which can be reduced in the UWS compared with WU (post-hoc test, $p < 0.001$).

The ANOVA results also show that UWS has little effect on knee moment, as shown in Figure 16(f–h). Compared with WU, the average knee moments over the whole stride and support phase (post-hoc test, $p = 0.93$, $p > 0.99$), and the peak knee moment (post-hoc test, $p = 0.08$) of UWS have no significant difference. However, compared with WU, the average knee moment over the support phase and the peak knee moment (post-hoc test, $p = 0.001$, $p = 0.005$) of UOS show that the knee moment is increased. As shown in Figure 16(j–l), compared with WU, the hip moment is reduced significantly in UWS, especially the peak hip moment (post-hoc test, $p = 0.03$).

4.3. Plantar pressure and spring compression

4.3.1. Plantar pressure and spring compression with 5 kg load

With 5 kg load, a similar trend can be observed from the vertical ground reaction forces among three conditions, as shown in Figure 17(a). Compared with WU, the vertical ground reaction force is reduced in

https://doi.org/10.1017/S026357472510249X Published online by Cambridge University Press

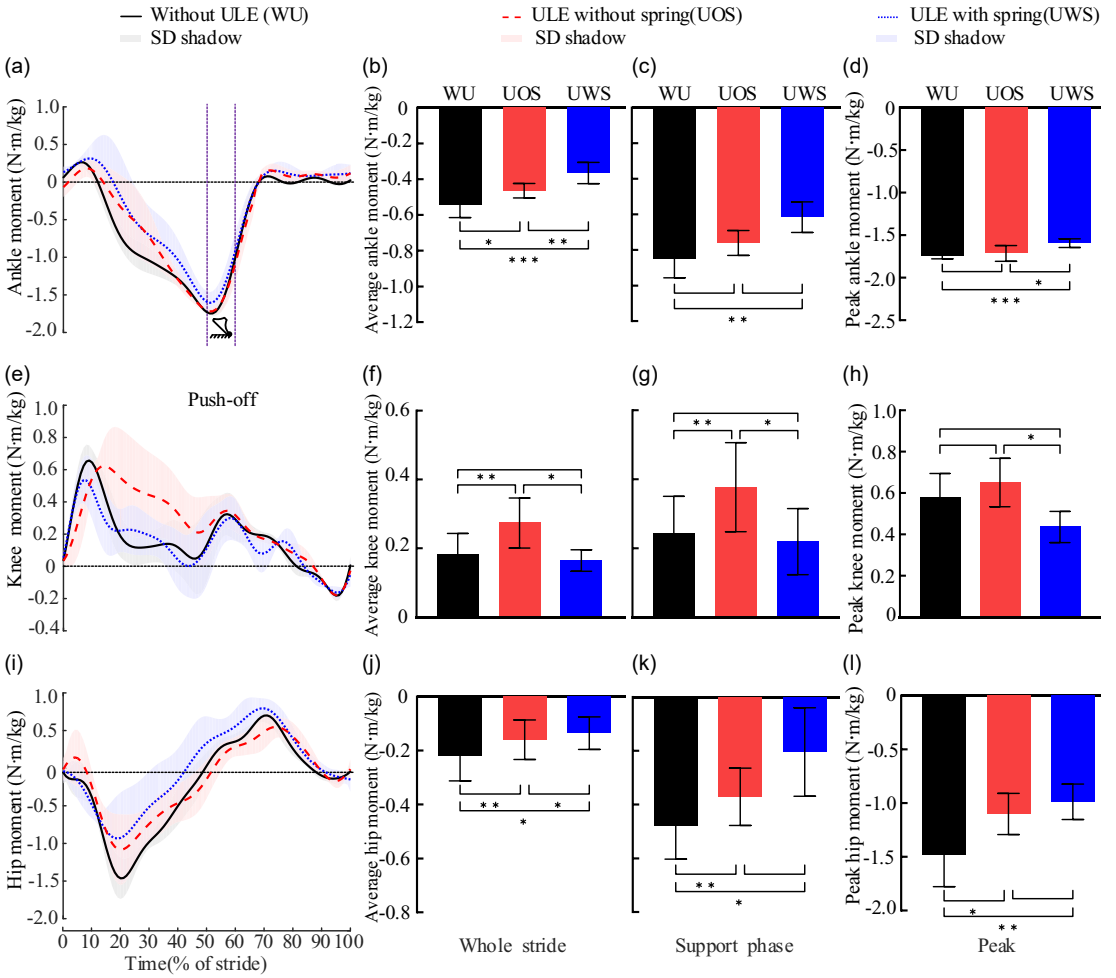


Figure 16. *Ankle, knee and hip joint moments with 20 kg load. (a–j) The meaning of the content in each figure is the same as that in Figure 13. Support phase, 0–68% stride.*

UWS, especially during the heel-pivot and toe-pivot stages. As shown in Figure 17(d), during the ankle-pivot stage, the spring is under maximum compression. However, during the toe-pivot stage, the spring is released. The ANOVA is performed for three conditions as shown in Figure 17(b) and (c). The average over the whole stride and peak vertical ground forces of three conditions show significant differences ($p = 0.001$, $p = 0.002$). Bonferroni post-hoc test shows that the average over the whole stride and the peak vertical ground forces can be reduced in the UWS compared with WU (post-hoc test, $p = 0.003$, $p = 0.02$).

4.3.2. Plantar pressure and spring compression with 5 kg load

With 10 kg load, a similar trend can be observed from the vertical ground reaction forces among three conditions, as shown in Figure 18(a). Compared with WU, the vertical ground reaction force is reduced in UWS, especially during the heel-pivot and toe-pivot stages. As shown in Figure 18(d), during the ankle-pivot stage, the spring is under maximum compression. However, during the toe-pivot stage, the spring is released. The ANOVA is performed for three conditions as shown in Figure 18(b) and (c). The average over the whole stride and peak vertical ground forces of three conditions show significant differences ($p = 0.004$, $p = 0.001$). Bonferroni post-hoc test shows that the average over the whole stride and the

https://doi.org/10.1017/S026357472510249X Published online by Cambridge University Press

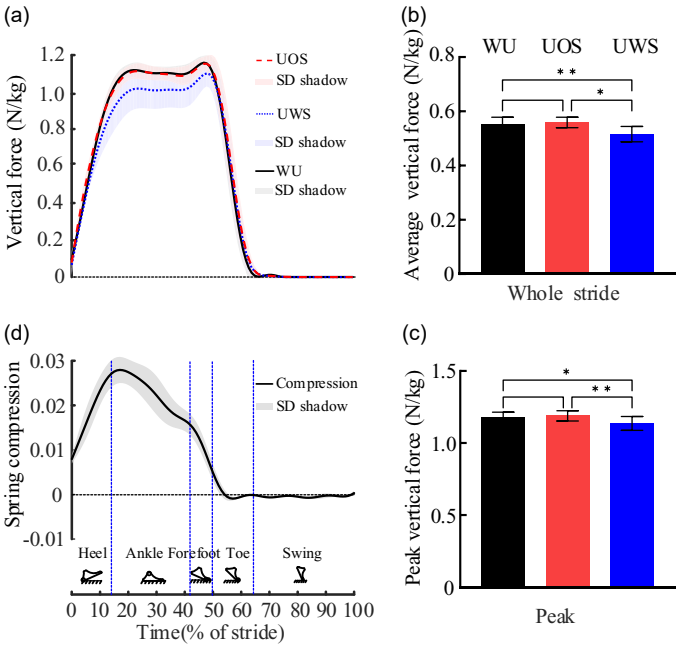


Figure 17. *Plantar pressure and spring compression with 5 kg load. (a,d) Trajectories of vertical ground reaction forces and spring compression averaged across subjects (N = 5), and shadows represent standard deviation (SD). (b,c) Average over the whole stride and peak vertical ground reaction force. *Significant difference at $p < 0.05$, **significant difference at $p < 0.01$, ***significant difference at $p < 0.001$; error bars, SD; all the force data were normalized to subject body mass; the spring data are normalized to subject body height.*

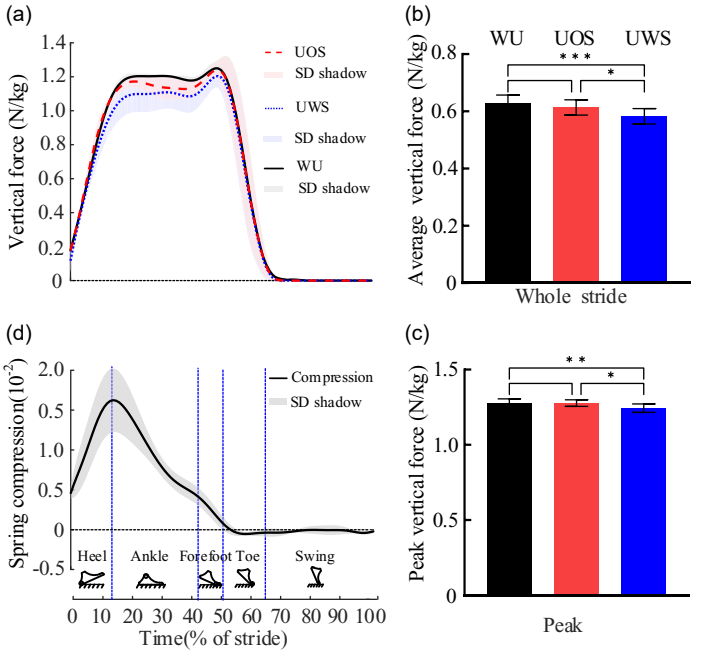


Figure 18. *Plantar pressure and spring compression with 10 kg load. (a–d) The meaning of the content in each figure is the same as that in Figure 17.*

https://doi.org/10.1017/S026357472510249X Published online by Cambridge University Press

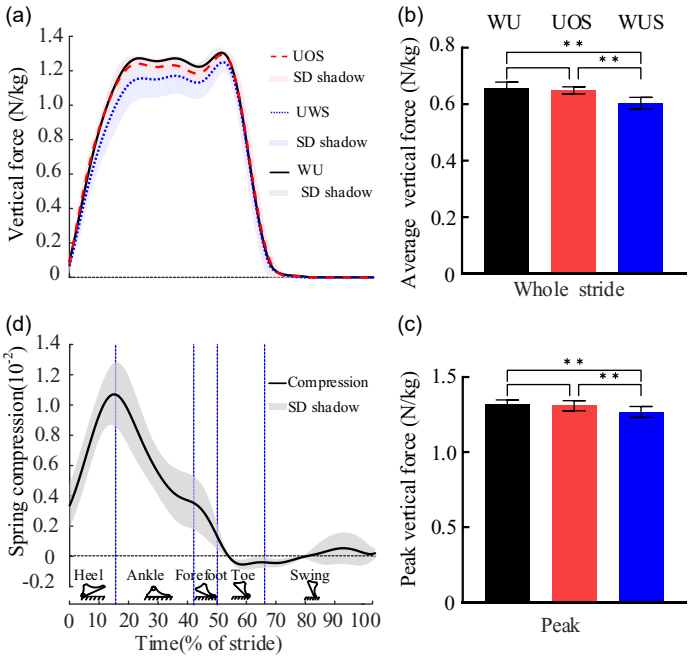


Figure 19. *Plantar pressure and spring compression with 15 kg load. (a–d) The meaning of the content in each figure is the same as that in Figure 17.*

peak vertical ground forces can be reduced in the UWS compared with WU (post-hoc test, $p < 0.001$, $p = 0.009$).

4.3.3. Plantar pressure and spring compression with 15 kg load

With 15 kg load, a similar trend can be observed from the vertical ground reaction forces among three conditions, as shown in Figure 19(a). Compared with WU, the vertical ground reaction force is reduced in UWS, especially during the heel-pivot and toe-pivot stages. As shown in Figure 19(d), during the ankle-pivot stage, the spring is under maximum compression. However, during the toe-pivot stage, the spring is released. The ANOVA is performed for three conditions as shown in Figure 19(b) and (c). The average over the whole stride and peak vertical ground forces of three conditions show significant differences ($p < 0.001$, $p < 0.001$). Bonferroni post-hoc test shows that the average over the whole stride and the peak vertical ground forces can be reduced in the UWS compared with WU (post-hoc test, $p = 0.004$, $p = 0.004$).

4.3.4. Plantar pressure and spring compression with 20 kg load

With 20 kg load, a similar trend can be observed from the vertical ground reaction forces among three conditions, as shown in Figure 20(a). Compared with WU, the vertical ground reaction force is reduced in UWS, especially during the heel-pivot and toe-pivot stages. As shown in Figure 20(d), during the ankle-pivot stage, the spring is under maximum compression. However, during the toe-pivot stage, the spring is released. The ANOVA is performed for three conditions as shown in Figure 20(b) and (c). The average over the whole stride and peak vertical ground forces of three conditions show significant differences ($p < 0.001$, $p < 0.001$). Bonferroni post-hoc test shows that the average over the whole stride and the peak vertical ground forces can be reduced in the UWS compared with WU (post-hoc test, $p < 0.001$, $p < 0.001$).

https://doi.org/10.1017/S026357472510249X Published online by Cambridge University Press

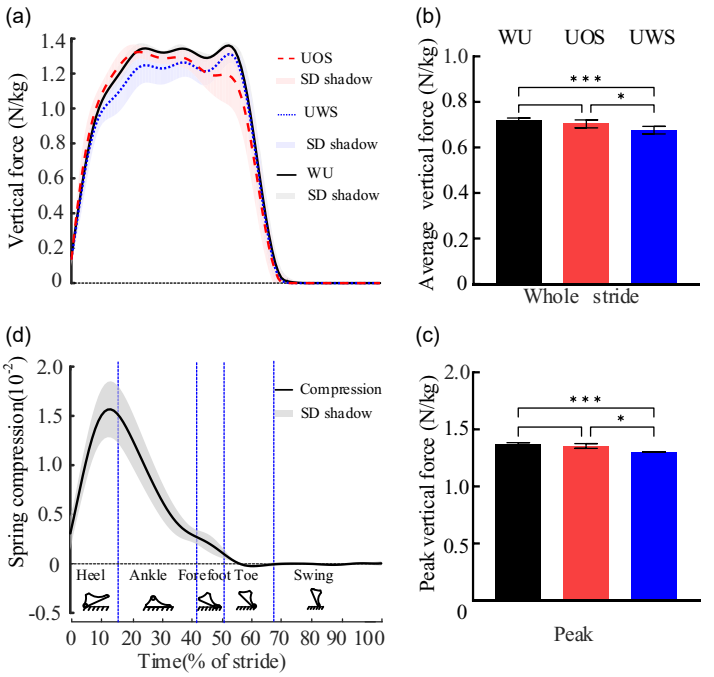


Figure 20. *Plantar pressure and springcompression with 20 kg load. (a–d) The meaning of the content in each figure is the same as that in Figure 17.*

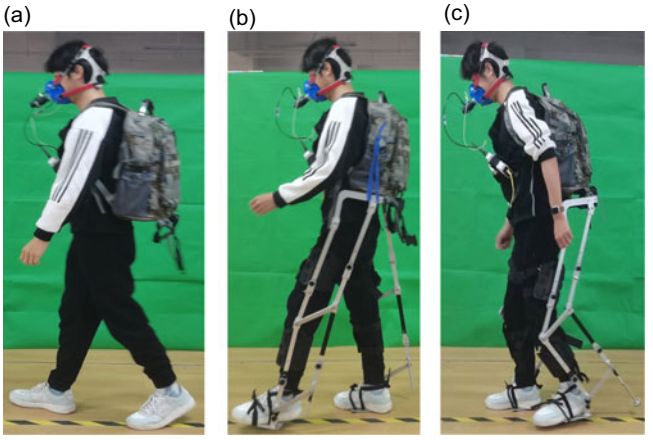


Figure 21. *Metabolic cost experiments. (a) WU. (b) UOS. (c) UWS.*

5. Metabolic cost experiment and result analysis

5.1. Metabolic cost experiment protocols

We conducted metabolic cost experiments on 5 healthy subjects carrying 5 loads (0, 5, 10, 15 and 20 kg) under three conditions, as shown in Figure 21. All subjects received explanations about the nature and possible consequences of the experiments before their participation. The study was approved by the Biomedical Ethics Committee of Hebei University of Technology. The ethics protocol number: HEBUTHMEC2025040.

The experiment consists of training and testing processes. All subjects, well-rested, must follow the training and testing processes. Colored squares denote different stages, each lasting 6 min, with stage

https://doi.org/10.1017/S026357472510249X Published online by Cambridge University Press

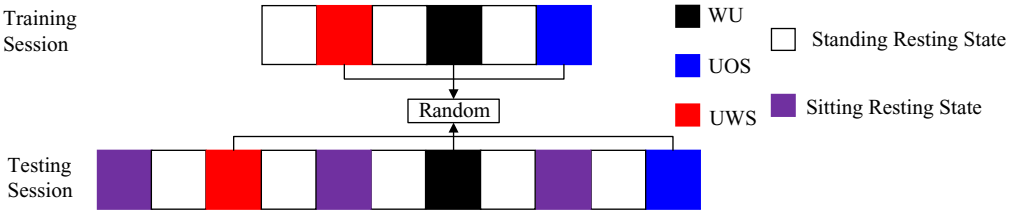


Figure 22. *Metabolic cost experiment protocol.*

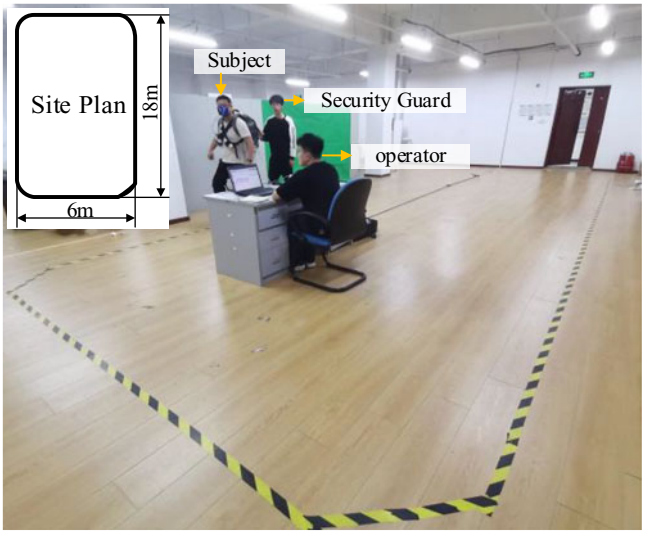


Figure 23. *Site plan and field experiment.*

descriptions provided in Figure 22. With the metronome, training and testing cadence were 60 steps/min, and the wearing condition of the exoskeleton and the load were randomly selected. During training, each subject completed 2 training sessions for each exoskeleton-wearing condition with each load. During testing, each subject completed 3 training sessions for each exoskeleton-wearing condition with each load. Each session should have a 20-min rest interval.

The site plan and field experiment are shown in Figure 23. During the experiment, a security guard held a metronome to supervise the gait cadence of the subjects while also ensuring safety protection. The operator was responsible for the overall experiment process and data recording.

The respiratory metabolic data of the subjects were collected using the cardiopulmonary exercise testing System (Oxycon Mobile, CareFusion, California, USA), as shown in Figure 24. Metabolic rate was estimated from average rates of oxygen consumption (VO_2) and carbon dioxide production (VCO_2) during the last 2 min in each experiment stage using a standard formula [43]. The metabolic rate during standing resting was subtracted from gross metabolic rate to get the net value attributable to the energetic demands of load-carrying under different exoskeleton-wearing conditions. Net metabolic rate values were then normalized to subject body mass.

The average and standard deviations of net metabolic rate values were calculated ($N = 5$) for each load under the three conditions. We used two-tailed paired t-test to compare the conditions of WU and UOS to identify the impact of ULE weight on human energy with 0 kg load. The average net metabolic rate values for each load (5, 10, 15, and 20 kg) under the three conditions were analyzed by one-way repeated measures ANOVA. Furthermore, the Bonferroni post hoc test was performed to determine the level of significant difference between conditions and verify the energy-saving effect of ULE with spring.

https://doi.org/10.1017/S026357472510249X Published online by Cambridge University Press

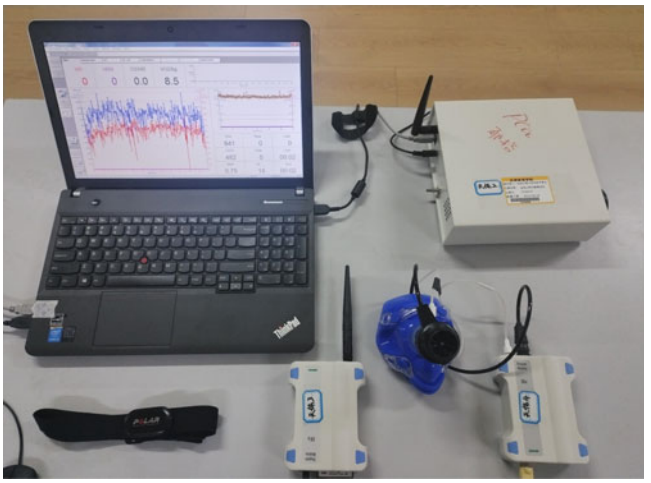


Figure 24. *The cardiopulmonary exercise testing system.*

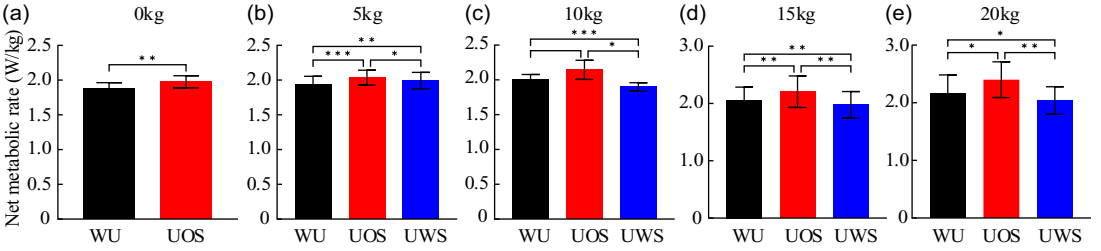


Figure 25. *Net metabolic rate under the three conditions. (a–e) Net metabolic rate of 0–20 kg load. *Significant difference at $p < 0.05$, **significant difference at $p < 0.01$, ***significant difference at $p < 0.001$; error bars, SD; all net metabolic rates were normalized to subject body mass.*

5.2. Results of metabolic cost experiments for energy-saving effect evaluation

With 0 kg load, compared with WU, the net metabolic rate is increased in UOS by 5.2 ± 1% (Mean ±SE, two-tailed paired t-test, $p = 0.007$), as shown in Figure 25(a). With 5 kg load, the ANOVA is performed for three conditions as shown in Figure 25(b). The net metabolic rates of three conditions show significant differences ($p < 0.001$). Bonferroni post-hoc test shows that the net metabolic rate is increased by 2.9 ± 0.5% (Mean±SE) in the UWS compared with WU (post-hoc test, $p = 0.007$). With 10 kg load, the ANOVA is performed for three conditions as shown in Figure 25(c). The net metabolic rates of three conditions show significant differences ($p = 0.01$). Bonferroni post-hoc test shows that the net metabolic rate is reduced by 5.6 ± 0.5% (Mean±SE) in the UWS compared with WU (post-hoc test, $p < 0.001$). With 15 kg load, the ANOVA is performed for three conditions as shown in Figure 25(d). The net metabolic rates of three conditions show significant differences ($p < 0.001$). Bonferroni post-hoc test shows that the net metabolic rate is reduced by 4.1 ± 0.7% (Mean±SE) in the UWS compared with WU (post-hoc test, $p = 0.005$). With 20 kg load, the ANOVA is performed for three conditions as shown in Figure 25(d). The net metabolic rates of three conditions show significant differences ($p < 0.001$). Bonferroni post-hoc test shows that the net metabolic rate is reduced by 5.9 ± 1.6% (Mean±SE) in the UWS compared with WU (post-hoc test, $p = 0.04$).

6. Discussion

Previous studies show that with the increase of the load, the spatiotemporal proportion of the double-support phase (heel-pivot and toe-pivot stages) in the gait cycle will also increase [27], which is verified

https://doi.org/10.1017/S026357472510249X Published online by Cambridge University Press

Table III. *Comparison of the energy reductions of different passive load-carrying exoskeletons.*

Study	Energyreduction	Load (kg)	Type & Structure	Exoskeleton weight (kg)	Speed (km/h)
Walsh et al.[19]	10% increase	36	Quasi-passiveknee variabledamper	11.7	3.31
Kim et al.[44]	30% increase20% increase3% decrease	01020	Passive4-Bar linkage Modular knee	–	2
This author	5.2% increase5.6% decrease5.9% decrease	01020	Passivedouble-support closed-chain	6.5	2.52

in the experiment of this paper. With 0, 5, 10, 15 and 20 kg load, the spatiotemporal proportions are 24%, 26%, 30%, 32% and 36%, respectively (Figure 14). The result shows that it is important to pay attention to the load-carrying assistance during the double-support phase. Meanwhile, the kinematics analysis also shows that wearing ULE with spring to carry load has less interference on human low limb motions.

In terms of joint moment assistance, compared with carrying 5, 10, 15 and 20 kg load by the human alone, wearing ULE with spring reduces the human average ankle moment over support phase by 36.8 ± 9.1%, 23.6 ± 3.9%, 33.4 ± 2.9% and 27.8 ± 3.4%, the peak ankle moment by 11.9 ± 1.6%, 11.2 ± 1.5%, 11.8 ± 1% and 8.7 ± 0.6% and the peak hip moment by 34.6 ± 8.2%, 14.3 ± 2.9%, 25.9 ± 5.6% and 33.3 ± 4.8% (Mean±SE), respectively. During the double-support phase, the peak hip moment is at the heel-pivot stage, and the peak ankle moment is at the toe-pivot stage. The reductions of the two peak moments indicate that wearing ULE with spring can provide joint moment assistance to the hip during collision execution and ankle during push-off execution. Furthermore, the reduction of average ankle moment over the whole support phase is greater than the peak reduction, indicating that wearing ULE with spring can also perform joint moment assistance to the ankle in the single-support phase.

In terms of support assistance, compared with carrying 5, 10, 15 and 20 kg load by the human alone, wearing ULE with spring reduces the human average vertical plantar pressure over the whole stride by 6.4 ± 0.7%, 7.2 ± 0.4%, 8.1 ± 1% and 6.1 ± 0.5%, the peak vertical plantar pressure by 3.7 ± 0.5%, 2.8 ± 0.4%, 3.8 ± 0.5% and 5.2 ± 0.3% (Mean±SE), respectively. During the double-support phase, the two peak vertical plantar pressures are at the beginning of the ankle-pivot and the toe-pivot stages. The reductions of the two peak vertical plantar pressures indicate that the posterior branch chain can perform support assistance during collision and push-off executions. Furthermore, compared with carrying load by the human alone, wearing ULE with spring reduces the average vertical plantar pressure over the whole support phase, indicating that ULE with spring can also perform support assistance in the single-support phase.

The analysis of the verification experiment results on the exoskeleton assisting effect shows that, compared with direct assistance to push-off of the following leg [33, 34], the support assistance of the guiding leg by the spring can reduce the collision, and then joint moment assistance can also be applied to the ankle moment of the following leg that is performing the push-off. Moreover, the ankle moment during the single-support phase is also reduced. One reason is that the support assistance of the posterior branch chain reduces the load bearing of human lower limbs; the other reason is that during the process from compression to release of the spring in the posterior branch chain, a forward force is generated on the anterior branch chain tightly bound to the human leg.

The analysis of the verification experiment results on the exoskeleton energy-saving effect results shows that, compared with the existing open-chain single-support lower limb exoskeletons [44], the closed-chain double-support configuration of ULE results in a lighter self-weight, and it exhibits better energy-saving performance when carrying heavy loads, as shown in Table III.

https://doi.org/10.1017/S026357472510249X Published online by Cambridge University Press

7. Conclusion

Based on the characteristics of the VPG during human load-carrying, this paper proposes a double-leg coordination principle for load-carrying assistance: assisting support of the guiding leg at the heel-pivot stage by the spring to reduce the collision, which can reduce the ankle moment of the following leg that is performing the push-off at the toe-pivot stage. A novel ULE with a double-support closed-chain configuration is designed. The results of experiments show that, during the double-support phase, ULE with spring can provide support assistance to the guiding leg and joint moment assistance to the ankle of the following leg; during the single-support phase, the process from compression to release of the spring in the posterior branch chain can also provide assistance to ankle moment of the supporting leg. Moreover, ULE with spring can perform support assistance over the whole support phase.

The metabolic cost experiment results show that ULE reduces human net metabolic rate under 10, 15 and 20 kg loads while providing joint moment and support assistance. Notably, no such reduction was observed with a 5 kg load, indicating a potential correlation among load, spring stiffness and energy consumption reduction – a focus for subsequent research. This study can also be applied to the powered exoskeleton for load-carrying assistance, providing a new avenue.

Author contribution. Jianjun ZHANG was in charge of the whole research; Cunjin AI wrote the manuscript and Jun WEI assisted with the analysis and validation. The remaining discussed and read the manuscript. All authors read and approved the final manuscript.

Financial support. This research work was supported by the National Natural Science Foundation of China Grant No.52405015, China Postdoctoral Science Foundation Funded Project No.2024M760729, the Central Government guides basic research projects of local science and Technology Development Funds Grant No.236Z1814G and the Scientific and Technological Program of Chongqing Municipal Education Commission Grant No.KJQN202401340.

Competing interests. The authors declare no conflicts of interest exist.

Ethical approval. The study was approved by the Biomedical Ethics Committee of Hebei University of Technology in Tianjin, China. The ethics protocol number: HEBUTHMEC2025040.

References

[1] B. Liew, S. Morris and K. Netto, "The effect of backpack carriage on the biomechanics of walking: A systematic review and preliminary meta-analysis," *J. Appl. Biomech.* **32**(6), 614–629 (2016).
[2] X. D. Qu and J. C. Yeo, "Effects of load carriage and fatigue on gait characteristics," *J. Biomech.* **44**(7), 1259–1263 (2011).
[3] D. M. Vickery-Howe, J. R. Drain, A. C. Clarke, B. J. Dascombe, J. T. McWilliam and K. J. Middleton, "Treadmill load carriage overestimates energy expenditure of overground load carriage," *Ergonomics* **64**(4), 521–531 (2021).
[4] J. F. Seay, "Biomechanics of load carriage-historical perspectives and recent insights," *J. Strength Cond. Res.* **29**(11), S129–S133 (2015).
[5] G. Walsh and D. C. Low, "Military load carriage effects on the gait of military personnel: A systematic review," *Appl. Ergon.* **93**(1), 103376 (2021).
[6] J. H. Park, X. Jin and S. K. Agrawal, "Second spine: Upper body assistive device for human load carriage," *J. Mech. Rob.* **7**(1), 11 (2015).
[7] J. H. Park, P. Stegall, H. H. Zhang and S. Agrawal, "Walking with a backpack using load distribution and dynamic load compensation reduces metabolic cost and adaptations to loads," *IEEE Trans. Neural Syst. Rehabil. Eng.* **25**(9), 1419–1430 (2017).
[8] K. N. Gregorczyk, L. Hasselquist, J. M. Schiffman, C. K. Bensel, J. P. Obusek and D. J. Gutekunst, "Effects of a lower-body exoskeleton device on metabolic cost and gait biomechanics during load carriage," *Ergonomics* **53**(10), 1263–1275 (2010).
[9] J. Zhu, Y. Wang, J. L. Jiang, B. Sun and H. Cao, "Unidirectional variable stiffness hydraulic actuator for load-carrying knee exoskeleton," *Int. J. Adv. Rob. Syst.* **14**(1), 1–12 (2017).
[10] A. B. Zoss, H. Kazerooni and A. Chu, "Biomechanical design of the berkeley lower extremity exoskeleton (BLEEX)," *IEEE/ASME Trans. Mechatron.* **11**(2), 128–138 (2006).
[11] L. M. Mooney and H. M. Herr, "Biomechanical walking mechanisms underlying the metabolic reduction caused by an autonomous exoskeleton," *J. Neuroeng. Rehabil.* **13**(4), 1–12 (2016).
[12] F. A. Panizzolo, I. Galiana, A. T. Asbeck, C. Siviy, K. Schmidt, K. G. Holt and C. J. Walsh, "A biologically-inspired multi-joint soft exosuit that can reduce the energy cost of loaded walking," *J. Neuroeng. Rehabil.* **13**(1), 43–56 (2016).

https://doi.org/10.1017/S026357472510249X Published online by Cambridge University Press

[13] Y. J. Zhan, W. J. Zhang, Z. M. Hou, R. J. Kang, J. S. Dai and Z. B. Song, "Non-anthropomorphic passive load-bearing lower-limb exoskeleton with a reconfigurable mechanism based on mechanical intelligence," *Mech. Mach. Theory* **201**, 105753 (2024).
[14] W. J. Zhang, Y. J. Zhan, W. J. Ju, Z. M. Hou, R. J. Kang, J. S. Dai and Z. B. Song, "A novel quasi-passive non-anthropomorphic lower limb exoskeleton for load-bearing," *IEEE Rob. Autom. Lett.* **9**(11), 9891–9898 (2024).
[15] M. Hao, J. W. Zhang, K. Chen, H. Asada and C. L. Fu, "Supernumerary robotic limbs to assist human walking with load carriage," *J. Mech. Rob.* **12**(6), 9 (2020).
[16] Z. Y. Liao, B. Chen, T. Z. Chang, Q. Zheng, K. M. Liu and J. N. Lv, "A human augmentation device design review: Supernumerary robotic limbs," *Ind. Rob.* **50**(2), 256–274 (2023).
[17] W. Fan, Z. Dai, B. Zhang, L. He, M. Pan, J. A. Yi and T. Liu, "HyExo: A novel quasi-passive hydraulic exoskeleton for load-carrying augmentation," *IEEE-ASME Trans. Mechatron.* **30**(1), 144–155 (2025).
[18] P. W. Kong, A. H. Koh, M. Y. M. Ho, M. N. S. Iskandar and C. X. E. Lim, "Effectiveness of a passive military exoskeleton in off-loading weight during static and dynamic load carriage: A randomised cross-over study," *Appl. Ergon.* **119**, 104293 (2024).
[19] C. J. Walsh, K. Endo and H. Herr, "A quasi-passive leg exoskeleton for load-carrying augmentation," *Int. J. Hum. Rob.* **4**(3), 487–506 (2007).
[20] J. Wei, S. Zhang and J. Zhang, "Biofusion design and parameter optimization for a novel passive assisted knee exoskeleton robot based on eight-bar mechanism," *Robotica* **42**(6), 1959–1985 (2024).
[21] H. Lim and S. Park, "Kinematics of lower limbs during walking are emulated by springy walking model with a compliantly connected, off-centered curvy foot," *J. Biomech.* **71**(1), 119–126 (2018).
[22] Y. Y. Tsai, W. C. Lin, K. Y. Cheng, J. Lee and T. Y. Lee, "Real-time physics-based 3D biped character animation using an inverted pendulum model," *IEEE Trans. Vis. Comput. Graph* **16**(2), 325–337 (2010).
[23] B. R. Whittington and D. G. Thelen, "A simple mass-spring model with roller feet can induce the ground reactions observed in human walking," *J. Biomech. Eng.* **131**(1), 011013 (2008).
[24] Y. Aoustin and A. M. Formalskii, "Walking of biped with passive exoskeleton: Evaluation of energy consumption," *Multibody Syst. Dyn.* **43**(1), 71–96 (2020).
[25] K. Kanjanapas and T. Masayoshi, "7 Degrees of Freedom Passive Exoskeleton for Human Gait Analysis: Human Joint Motion Sensing and Torque Estimation during Walking In," *6th IFAC Symposium on Mechatronic Systems* (ELSEVIER, Hangzhou, China, 2013) pp. 285–292.
[26] H. Kazerooni, J. L. Racine, L. Huang and R. Steger, "On the Control of the Berkeley Lower Extremity Exoskeleton (BLEEX)," IEEE International Conference on Robotics and Automation (ICRA) (IEEE, Barcelona, SPAIN, 2006) pp. 4353–4360.
[27] T. Huang and A. D. Kuo, "Mechanics and energetics of load carriage during human walking," *J. Exp. Biol.* **217**(4), 605–613 (2014).
[28] A. H. Hansen, D. S. Childress and E. H. Knox, "Roll-over shapes of human locomotor systems: Effects of walking speed," *Clin. Biomech.* **19**(4), 407–414 (2004).
[29] A. S. Levens, V. T. Inman and J. A. Blosser, "Transverse rotation of the segments of the lower extremity in locomotion," *J. Bone Joint Surg.* **30**(4), 859–872 (1948).
[30] C. J. Ai, J. Wei, J. J. Zhang, J. K. Song, W. L. Lv and C. L. Liu, "Variable pivot gait based a novel dynamics correction method for human lower limbs model," *J. Biomech. Eng.-Trans. ASME* **146**(4), 10 (2024).
[31] F. Doerks, L. Riedel, A. K. Einfeldt, H. Windhagen, C. Hurschler and E. Jakubowitz, "Contribution of various forefoot areas to push-off peak at different speeds and slopes during walking," *Gait Posture* **108**(1), 264–269 (2024).
[32] D. A. Winter, "Energy generation and absorption at the ankle and knee during fast, natural, and slow cadences," *Clin. Orthop. Relat. Res.* **175**(175), 147–154 (1983).
[33] S. H. Collins, M. B. Wiggin and G. S. Sawicki, "Reducing the energy cost of human walking using an unpowered exoskeleton," *Nature* **522**(7555), 212–215 (2015).
[34] X. Y. Wang, S. Guo, B. J. Qu, M. J. Song and H. B. Qu, "Design of a passive gait-based ankle–foot exoskeleton with self-adaptive capability," *Chin. J. Mech. Eng.* **33**(3), 1–11 (2020).
[35] C. H. Soo and J. M. Donelan, "Coordination of push-off and collision determine the mechanical work of step-to-step transitions when isolated from human walking," *Gait Posture* **35**(2), 292–297 (2012).
[36] K. E. Zelik, K. Z. Takahashi and G. S. Sawicki, "Six degree-of-freedom analysis of hip, knee, ankle and foot provides updated understanding of biomechanical work during human walking," *J. Exp. Biol.* **218**(6), 876–886 (2015).
[37] W. H. Ho, T. Y. Shiang, C. C. Lee and S. Y. Cheng, "Body segment parameters of young Chinese men determined with magnetic resonance imaging," *Med. Sci. Sports Exercise* **45**(9), 1759–1766 (2013).
[38] M. G. Hoy, F. E. Zajac and M. E. Gordon, "A musculoskeletal model of the human lower extremity: The effect of muscle, tendon, and moment arm on the moment–angle relationship of musculotendon actuators at the hip, knee, and ankle," *J. Biomech.* **23**(2), 157–169 (1990).
[39] S. L. Delp, F. C. Anderson, A. S. Arnold, P. Loan and D. G. Thelen, "OpenSim: Open-source software to create and analyze dynamic simulations of movement," *IEEE Trans. Bio-MED Eng.* **54**(11), 1940–1950 (2007).
[40] A. Falisse, G. Serrancolí, C. L. Dembia, J. Gillis and F. D. Groote, "Algorithmic differentiation improves the computational efficiency of OpenSim-based trajectory optimization of human movement," *PLOS ONE* **14**(10), e0217730 (2019).
[41] J. Antonie, D. Blana and H. Dieter, "Implicit methods for efficient musculoskeletal simulation and optimal control," *Proc. IUTAM* **2**(1), 297–316 (2011).

https://doi.org/10.1017/S026357472510249X Published online by Cambridge University Press

[42] F. De Groote, A. L. Kinney, A. V. Rao and B. J. Fregly, "Evaluation of direct collocation optimal control problem formulations for solving the muscle redundancy problem," *Ann. Biomed. Eng.* **44**(10), 2922–2936 (2016).
[43] D. R. Westenskow, C. A. Schipke, J. L. Raymond, J. R. Saffle, J. M. Becker, E. W. Young and C. A. Cutler, "Calculation of metabolic expenditure and substrate utilization from gas exchange measurements," *Jpen J. Parenteral Enteral Nutr.* **12**(1), 20 (1988).
[44] H. J. Kim, D. H. Lim, W. S. Kim, C. S. Han, "Development of a passive modular knee mechanism for a lower limb lxoskeleton robot and its effectiveness in the workplace," *Int. J. Precis. Eng. Manuf.* **21**(2), 227–236 (2020).

Cite this article: C. Ai, J. Zhang, J. Wei, J. Song, C. Liu and A. Shi (2025). "Configuration design and assisting effect evaluation of a novel double-support closed-chain unpowered load-carrying exoskeleton based on variable pivot gait", Robotica **43**, 3657–3681. https://doi.org/10.1017/S026357472510249X

https://doi.org/10.1017/S026357472510249X Published online by Cambridge University Press